RSC Advances

PAPER

View Article Online
View Journal | View Issue



Cite this: *RSC Adv.*, 2023, **13**, 22815

# Mesoporous sol–gel silica supported vanadium oxide as effective catalysts in oxidative dehydrogenation of propane to propylene

Xin-Peng Guo, Xiao-Xiao Wang, Hai-Qiang LU and Zhen-Min Liu*

Received 15th June 2023
Accepted 14th July 2023

DOI: 10.1039/d3ra04024k

rsc.li/rsc-advances

Vanadium oxide incorporated mesoporous silica (V-m-$SiO_2$) were designed and synthesized using a surfactant-modified sol–gel method. Detailed characterization shows that monomeric [$VO_4$] sites containing one terminal V=O bond and three V–O-support bonds are dominated until atomic ratio of vanadium to silicon approaches to 5%. It is also confirmed that such V-m-$SiO_2$ catalyst contains high proportion of vanadium oxide species interacting strongly with silica. Compared to vanadium oxide supported mesoporous silica (V/m-$SiO_2$) prepared using a traditional impregnation method, present V-m-$SiO_2$ catalyst exhibits more superior ability to catalyze oxidative dehydrogenation of propane to propylene. By correlation with structural data, superior catalytic performance of present V-m-$SiO_2$ catalyst can be reasonably attributed, in part, to its favorable geometric and electronic properties rendered by the unique preparation method.



## 1. Introduction

Catalytic dehydrogenation of propane to propylene, one of most important feeds in chemical industry, supplies ~10% of the global propylene production capacity, but it practically suffers from the thermodynamic limitation in further prompting the reaction efficiency and also the rapid catalyst deactivation by coking and catalyst sintering that requires a frequent regeneration of the catalysts under harsh conditions.[1–3] As an alternative to industrialized propane dehydrogenation, oxidative dehydrogenation of propane to generate propylene, with the prominent characters of free coking of catalyst and non-equilibrium limit in propane conversion, has always been the focus of the researchers' attention.[4–6]

In the past few decades, supported vanadium oxide catalysts show the most promising reactivity for oxidative dehydrogenation of propane since the favorable redox properties of active vanadium sites.[7,8] However, selectivity to propylene remains too low to be commercially attractive even at moderate propane conversion since electron-rich olefin easily reacts with the surface of metal oxide catalysts, resulting in the cleavage the C–C bond through a consecutive oxygen insertion and thus forming the undesired over-oxidation product $CO_x$.[9–16] As an example, at 20% propane conversion, a typical value of industrial interest, the selectivity to propylene typically drops to less than 60%.

For supported vanadium oxide catalysts, it is commonly agreed that vanadium oxide can be present on the support oxide in three distinct forms: *i.e.* as monomeric vanadia species at low loadings, as oligomeric form at medium loadings, and as $V_2O_5$ crystals at high loadings.[17–19] The existing state of vanadium and thus the catalytic behavior of supported vanadium oxide catalysts is influenced by the specific surface area, vanadium content, and the composition of the support.[20–23] Mesoporous silica is considered a suitable support of dispersing vanadium to catalyze oxidative dehydrogenation of propane due to its available surface area, nanoporous space and relative inertness, which are in favor of the rapid desorption of the electron-rich propylene to avoid deep oxidation.[24,25] However, for silica supported vanadium oxide catalysts, the transition from monomeric to crystalline $V_2O_5$ nanoparticles (>3 nm), accompanied by the decay of catalytic reactivity of vanadium-based catalysts in oxidative dehydrogenation of propane, occurs easily even at a sub-monolayer coverage,[17,26] and therefore, in order to improve the catalytic activity and stability, there is an urgent need to develop new synthesis methods to enhance an interaction of vanadium oxide with silica for optimizing the dispersed state of vanadium on silica.

Herein, we report an enhanced effect of interaction between vanadium oxide and silica as exemplified by using a surfactant-modified sol–gel method to prepare vanadium oxide incorporated mesoporous silica (V-m-$SiO_2$). Compared to vanadium oxide supported mesoporous silica prepared by a traditional impregnation method, V-m-$SiO_2$ allows for larger vanadium dispersion as well as stronger interaction between vanadium oxide and silica, and thereby promoting the catalytic performance in oxidative dehydrogenation of propane. This is demonstrated by combing the evaluating results of catalytic behavior with a variety of characterization techniques, including X-ray diffraction, nitrogen physisorption, high-resolution transmission electron microscopy, Raman

*College of Chemical Engineering and Technology, Taiyuan University of Science and Technology, Taiyuan 030024, China. E-mail: zhmliu@tyust.edu.cn*

spectroscopy, diffuse reflectance UV-vis spectroscopy, and X-ray photoelectron spectroscopy.

## 2. Experimental

### 2.1 Catalyst preparation

Initially, mesoporous silica (denoted as m-$SiO_2$) and vanadium oxide incorporated mesoporous silica (denoted as $x$% V-m-$SiO_2$), where $x$% represents the V/Si atomic ratio in the catalyst, were synthesized using a surfactant-modified sol–gel method.[27–29] On the one hand, the fine control of the sol–gel process can come true the atom-level cross-linking between silicon and vanadium precursors, and on the other hand, the creation of the ordered mesoporous structure is of advantage to improve the accessibility of active species.

Specifically, m-$SiO_2$ support and $x$% V-m-$SiO_2$ catalysts were prepared as follows: (i) 1.0 g of tri-block copolymers ($EO_{20}$-$PO_{70}EO_{20}$, $M = 5800$) and 0.10 mL of hydrochloric acid (HCl, 12 M) were mixed with 20.0 mL of ethanol; (ii) a pre-hydrolyzed solution of tetraethoxysilane (TEOS, $\geq$ 98.0%) was prepared by fluxing an ethanol solution (5 mL) containing 10.0 mmol of TEOS, 20.0 mmol of distilled water and $5.5 \times 10^{-3}$ mmol of HCl for 90 min at 353 K; (iii) an ethanol solution (10 mL) containing 0.30 mmol of vanadium(v) trichloride oxide ($OVCl_3$, $V^{5+}$ 28.5%) was stirred at room temperature for 5 min; (iv) the above solutions were mixed and stirred for 10 min at room temperature. The resulting mixture was then poured into a dish ($\phi$120 mm); (v) the solvent was evaporated at 313 K with relative humidity of 40–60%. After 24 hours, a transparent film was formed, which was then aged at 353 K for additional 48 hours; and (vi) finally, the as-prepared solid product was calcined at 833 K for 6 hours (temperature ramp rate at 1 K $min^{-1}$) to remove templates. For comparison, a supported catalyst (denoted as 3% V/m-$SiO_2$) was also prepared by impregnating m-$SiO_2$ with an aqueous solution of ammonium metavanadate at 353 K for 24 hours, followed by drying and calcining in air at 833 K for 3 hours.

### 2.2 Catalyst characterization

X-ray diffraction (XRD) analysis was carried out using a Panalytical X'pert PRO X-ray diffractometer. Cu-$K_\alpha$ radiation obtained at 40 kV and 30 mA was used as the X-ray source. The small-angle XRD patterns were used to determine structural quality and symmetry, and wide-angle XRD patterns were recorded for the phase analysis.

Brunauer–Emmett–Teller (BET) surface area and pore volume of the catalysts were measured by nitrogen physisorption at 77 K using a Micromeritics Tristar 3000 instrument. The pore size of the catalysts was calculated by the BJH model based on the adsorption curve. Before the measurement, the samples were degassed at 573 K for 2 hours.

Microstructure of the catalysts was investigated using a Tecnai F30 high-resolution transmission electron microscope (FHI Company) operated at an accelerating voltage of 300 kV.

The dehydrated Raman spectroscopy were recorded using a Renishaw 1000 system equipped with a CCD detector and a Leica DMLM microscope. A laser $\lambda = 532$ nm was used as the excitation source. The samples were pressed into tablets and placed in the cell and then directly heated up to 773 K under flowing synthetic air.

UV-visible diffuse reflectance (UV-vis DRS) spectroscopy was performed with a Varian-Cary 5000 spectrometer equipped with a diffuse-reflectance accessory. The spectra were collected in the range 200–800 nm at room temperature. The samples were dehydrated at 723 K for 3 hours before the UV-vis DRS measurements.

X-ray photoelectron spectroscopy (XPS) analysis was carried out with a Quantum 2000 Scanning ESCA Microprobe instrument (Physical Electronics) using Al $K_\alpha$ radiation as the X-ray source. Sample for XPS analysis was prepared by pressing the catalyst powder into a self-supported disk at 4 MPa. The disk was then calcined at 723 K for 3 hours before the measurement. The binding energy (BE) of the element was calibrated using a Si 2p photoelectron peak at 103.2 eV.

### 2.3 Catalytic test

A fixed-bed reactor was used to test the catalytic performances of propane oxidative dehydrogenation at atmospheric pressure. A gas mixture with a molar ratio of 16.8 kPa $C_3H_8$, 16.8 kPa $O_2$ and $N_2$ balance and total flow rate of 60 mL $min^{-1}$ passed through the catalyst bed at temperature of 733–813 K. The reactants and products were analyzed using an on-line gas chromatograph.

Conversion was defined as the number of moles of carbon converted divided by the number of moles of carbon present in the feed. Specific site rates ($TOF_{C_3H_8}$, millimoles of propane converted per mole of V per second) of propane conversion were evaluated assuming that all vanadium elements participate in converting process of propane. Selectivity was defined as the number of moles of carbon in the product divided by the number of moles of carbon reacted. Detailed calculation as follows:

$$\text{Conversion}\ (\%) = \{[(F_{in}(C_3H_8) - F_{out}(C_3H_8)]/F_{in}(C_3H_8)\} \times 100$$

$$\text{Selectivity}\ (\%) = [(n_i/3) \times (F_{out}(i))]/\Sigma i[(n_i/3) \times (F_{out}(i))] \times 100$$

where $i$ represents hydrocarbon products in the effluent gas stream, $n_i$ is the number of carbon atoms of component $i$, and $F(i)$ is the corresponding flow rate.

## 3. Results and discussion

### 3.1 Structural analysis of m-$SiO_2$ support and V-containing m-$SiO_2$ catalysts

The mesostructure of m-$SiO_2$ support, series of $x$% V-m-$SiO_2$ catalysts, and referenced 3% V $m^{-1}$-$SiO_2$ catalyst was characterized by small-angle XRD, $N_2$ physisorption and HR-TEM measurements. As shown in Fig. 1a, the small-angle XRD patterns of m-$SiO_2$ support and V-containing m-$SiO_2$ catalysts show one well-resolved diffraction peak in the range of 1–1.5°, which can be assigned to the (100) reflection associated with *P 6mm* symmetry, suggesting that these catalysts have a typical two-dimensional hexagonal mesoporous structure.[30] The well-

 

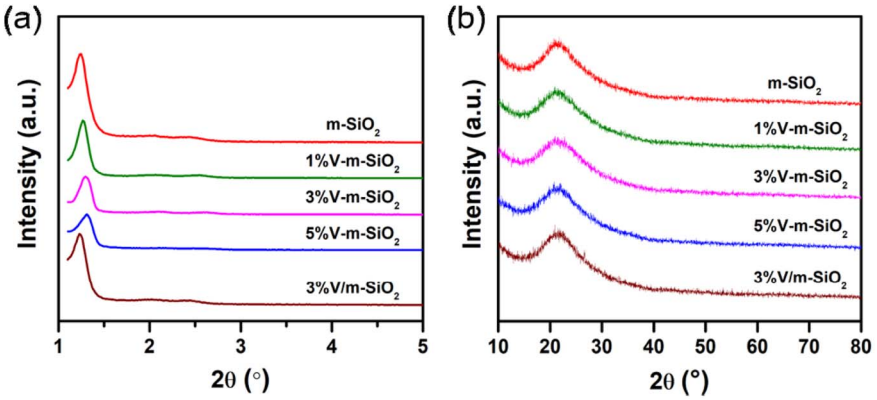


Fig. 1 Small-angle (a) and wide-angle (b) XRD patterns of m-$SiO_2$ support, series of *x*% V-m-$SiO_2$ catalysts, and referenced 3% V/m-$SiO_2$ catalyst.

Table 1 Structural parameters of m-$SiO_2$ support and V-containing m-$SiO_2$ catalysts

| Samples[a] | BET surface area $S_{BET}$/$m^2$ $g^{-1}$ | Pore volume $V_{total}$/$cm^3$ $g^{-1}$ | BJH pore size $D_{BJH}$/nm | Lattice spacing $d_{100}$/nm | Wall thickness[b] $\delta$/nm |
|---|---|---|---|---|---|
| m-$SiO_2$ | 283 | 0.46 | 6.4 | 7.1 | 3.6 |
| 1% V-m-$SiO_2$ | 268 | 0.45 | 6.1 | 6.9 | 3.7 |
| 3% V-m-$SiO_2$ | 217 | 0.42 | 5.9 | 6.7 | 3.6 |
| 5% V-m-$SiO_2$ | 209 | 0.41 | 5.9 | 6.7 | 3.6 |
| 3% V $m^{-1}$-$SiO_2$ | 232 | 0.40 | 5.8 | 7.2 | 4.4 |

[a] Atomtic percentage of vanadium to silicon. [b] $\delta = 2 \times d_{100}/3^{1/2} - D_{BJH}$.

ordered hexagonal arrays of mesopore channels were further confirmed by HR-TEM images of representative 3% V-m-$SiO_2$ (Fig. 3a) and 3% V/m-$SiO_2$ (Fig. 3c) catalysts. According to the data of small-angle XRD measurement, lattice spacing values of (100) reflections (*i.e.*, $d_{100}$, Table 1) of m-$SiO_2$, 1% V-m-$SiO_2$, 3% V-m-$SiO_2$ and 5% V-m-$SiO_2$ catalysts were determined to be 7.1 nm, 6.9 nm, 6.7 nm, and 6.7 nm, respectively. Compared to that of m-$SiO_2$, the $d_{100}$ values of the V-containing m-$SiO_2$ catalysts prepared by the modified sol–gel method become smaller, indicating a lattice contraction. Whereas for a supported 3% V/m-$SiO_2$ catalyst, the $d_{100}$ value (Table 1) has an increase of 0.1 nm in comparison to 7.1 nm of m-$SiO_2$ support.

Mesoporous characteristics of m-$SiO_2$ support, series of *x*% V-m-$SiO_2$ catalysts, and supported 3% V/m-$SiO_2$ catalyst were also characterized *via* $N_2$ physisorption measurement. Fig. 2 gives the adsorption–desorption isotherms of nitrogen and the BJH pore size distribution plots of series of samples. As observed in Fig. 2a, all the samples show a jump of adsorbed volume in the $P/P_0$ range of 0.5–0.7, and meanwhile present the

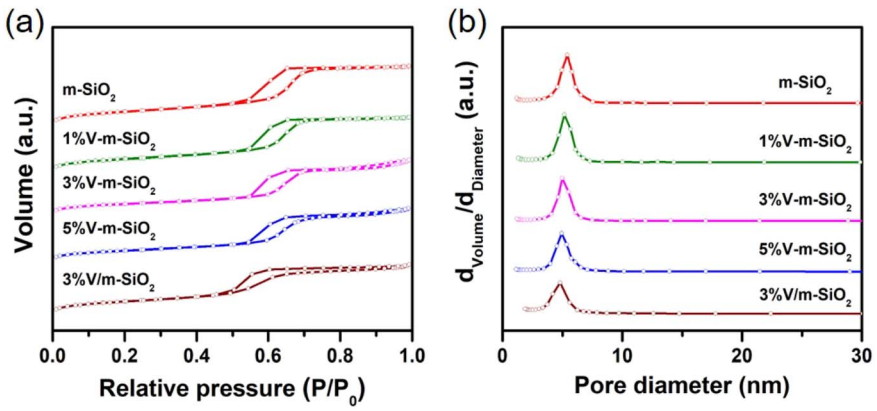


Fig. 2 $N_2$ adsorption–desorption isotherms (a) and BJH pore size distribution plots (b) of m-$SiO_2$ support, series of *x*% V-m-$SiO_2$ catalysts, and referenced 3% V/m-$SiO_2$ catalyst.

large hysteresis loops in this region, indicating a type IV isotherm, which is characteristic of ordered mesoporous materials. The pore size plots, calculated from the isotherm using the BJH model, exhibits the sharp distribution around the size of ~6 nm (Fig. 2b), indicating the presence of ordered mesopores in these samples, which is coincident with the measured results of the XRD patterns and HR-TEM images. Furthermore, the detailed pore parameters are summarized in Table 1. From Table 1, one can see that all the samples exhibit the comparable BET surface area (200–300 $m^2\ g^{-1}$) and pore volume (0.4–0.5 $cm^3\ g^{-1}$). Both high surface area and large pore volume further support the fact that these samples have typical mesoporous structure. It is noted that average pore sizes of all the V-containing m-$SiO_2$ catalysts ($x$% V-m-$SiO_2$ and 3% V/m-$SiO_2$) are smaller than that of m-$SiO_2$ support (Table 1 and Fig. 2b). Combined with the results of XRD analysis, pore wall thickness of all the samples was calculated by subtracting pore size from unit cell parameters obtained by $2 \times d_{100}/3^{1/2}$.[30] As exhibited in the last column in Table 1, series of $x$% V-m-$SiO_2$ prepared by the modified sol–gel method possess a pore wall of ~3.6 nm, while thicker pore wall (4.4 nm) is present in supported 3% V/m-$SiO_2$ catalyst.

### 3.2 Local structure of active vanadium species dispersed into m-$SiO_2$

To identify the phase state of active vanadium species in series of $x$% V-m-$SiO_2$ catalysts and supported 3% V-m-$SiO_2$ catalyst, the wide-angle XRD measurements were performed and the resulting XRD patterns were presented in Fig. 1b. The $x$% V-m-$SiO_2$ catalysts prepared by the modified sol–gel method only show the broad diffraction peak, which can be assigned to amorphous silica phase, and no diffraction peaks corresponding to vanadium-containing crystalline phase are observed until the content of vanadium reaches 5%, revealing the highly-dispersed state of vanadium species in mesoporous silica matrix. Furthermore, at the nanometer scale, the HAADF-STEM imaging combined with EDX element-mapping analysis was carried out to probe the phase state of active vanadium species. Fig. 3b shows the HAADF-STEM image of representative 3% V-m-$SiO_2$ catalyst and the elemental mappings of same region, with different colors denoting three elements (orange: silicon, red: oxygen, green: vanadium). In the HAADF-STEM image, few large-sized crystalline species were observed, suggesting the highly-dispersed nature of vanadium species in the mesoporous silica matrix, in agreement with the results of wide-angle XRD analysis. Comparing the maps of silicon, oxygen and vanadium elements, one can see that vanadium species, at least at the nanoscale, are homogeneously dispersed throughout mesoporous silica matrix.

Furthermore, comprehensive spectroscopic techniques involving in Raman spectroscopy, UV-vis DRS spectroscopy and XPS spectroscopy were used to molecule-level clarify both geometric and electronic structure of active vanadium species in series of $x$% V-m-$SiO_2$ catalysts and supported 3% V/m-$SiO_2$ catalyst. Fig. 4a presents the Raman spectra in the range of 400–1200 $cm^{-1}$ of 1% V-m-$SiO_2$, 3% V-m-$SiO_2$, 5% V-m-$SiO_2$ and

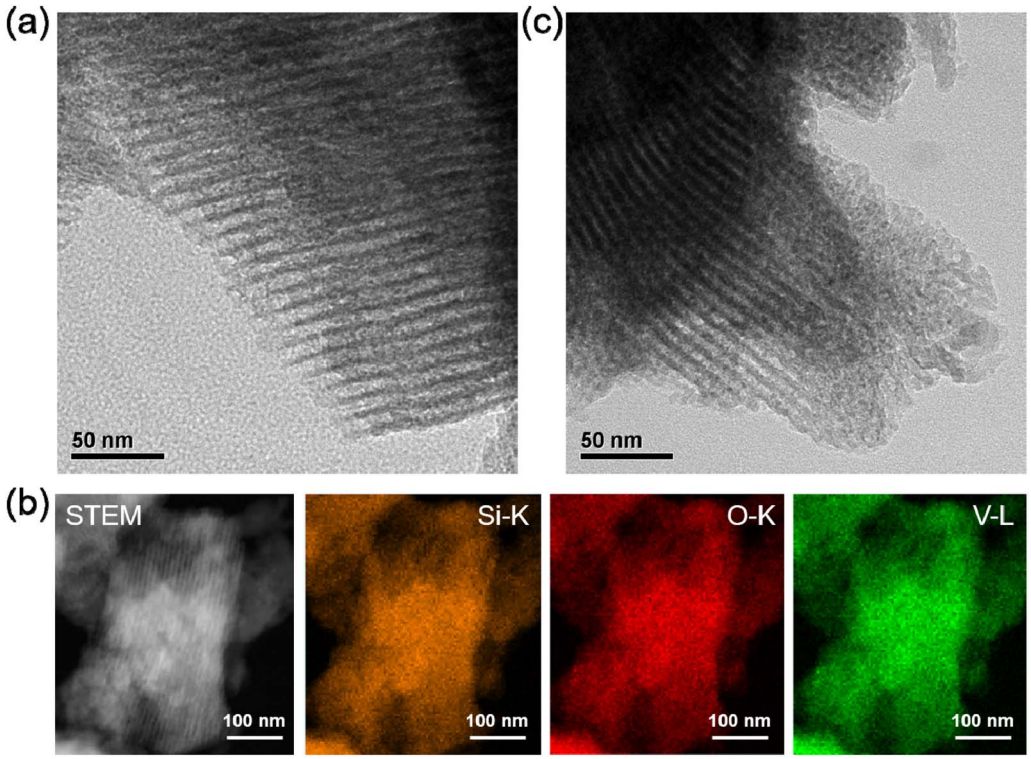


Fig. 3 The HR-TEM images of 3% V-m-$SiO_2$ (a) and 3% V/m-$SiO_2$ (c), and HAADF-STEM images and EDX element-mapping analysis (b) of 3% V-m-$SiO_2$ sample.

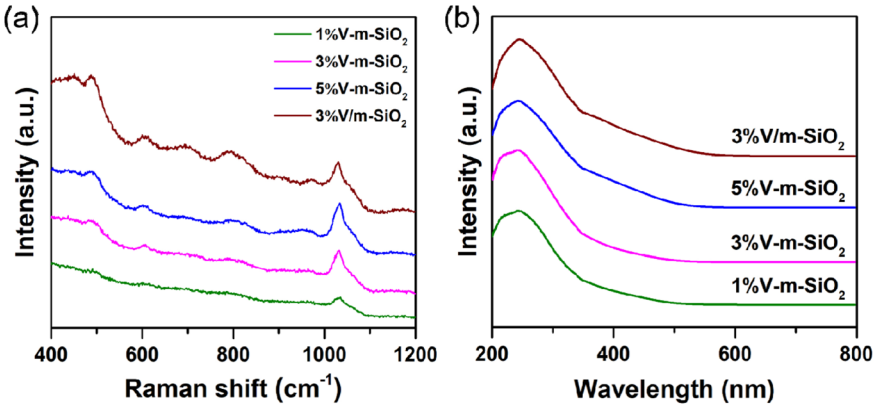


Fig. 4 Raman spectroscopy (a) and UV-vis DRS spectroscopy (b) of series of *x*% V-m-$SiO_2$ catalysts and referenced 3% V/m-$SiO_2$ catalyst under dehydrated conditions.

supported 3% V/m-$SiO_2$ catalysts under dehydrated conditions. For all the V-containing catalysts, no crystalline $V_2O_5$ (996 $cm^{-1}$) is detected in the Raman spectra, which is consistent with the absence of $V_2O_5$ diffraction peak in the XRD pattern. All the spectra of V-containing catalysts show a strong Raman signal at 1035 $cm^{-1}$ which can be attributed to the symmetric stretching mode of vanadyl (V=O) bonds, indicating the presence of monomeric $VO_4$ species in tetrahedral coordination [O=V–$(OSi)_3$] on the surface of support.[31–33] Moreover, for series of *x*% V-m-$SiO_2$ catalysts prepared *via* a modified sol–gel method, the intensity of Raman signal at 1035 $cm^{-1}$ is positively correlated with vanadium content. When vanadium content increases to 3%, the signal of the monomeric band becomes prominent, and further increases to 5%, the signal continuously enhances, suggesting that monomeric $VO_4$ species remain be dominated in these catalysts even if vanadium content reaches 5%. Whereas, for supported 3% V/m-$SiO_2$ catalyst, except for a strong band at 1035 $cm^{-1}$, another band at 698 $cm^{-1}$ with visible intensity is observed. This band can be assigned to the stretching motions of oxygen in a bridging position between three vanadium atoms [$OV_3$],[18] suggesting the presence of polymeric vanadia species in supported 3% V/m-$SiO_2$ catalyst prepared by traditional impregnation method. That is to say, a modified sol–gel method can endow high dispersion of vanadium oxide species.

The UV-vis DRS spectra (Fig. 4b) of both 1% V-m-$SiO_2$ and 3% V-m-$SiO_2$ catalysts exhibit one charge transfer (CT) band at ~242 nm, and one shoulder at ~300 nm. The CT band at ~240 nm and the shoulder at ~300 nm suggested the presence of two different kinds of tetrahedral $V^{5+}$ center, strongly and less distorted, respectively.[34] For supported 3% V/m-$SiO_2$ catalyst, one new shoulder band appears at ~400 nm, corresponding to octahedral $V^{5+}$ ion, indicates the presence of polymerized vanadium species.[35] These results mean that the existent forms of vanadium species in mesoporous silica matrix are diverse, nevertheless, the highly-dispersed state is dominant, which is consistent with the Raman results.

The XPS analyses were implemented to investigate the chemical states of vanadia species dispersed in mesoporous silica. The $V_{2p3/2}$, $Si_{1s}$ and $O_{1s}$ XPS spectra of 1% V-m-$SiO_2$, 3% V-m-$SiO_2$, 5% V-m-$SiO_2$ and 3% V $m^{-1}$-$SiO_2$ catalysts are presented in Fig. 5. For series of *x*% V-m-$SiO_2$ catalysts, the XPS spectra of

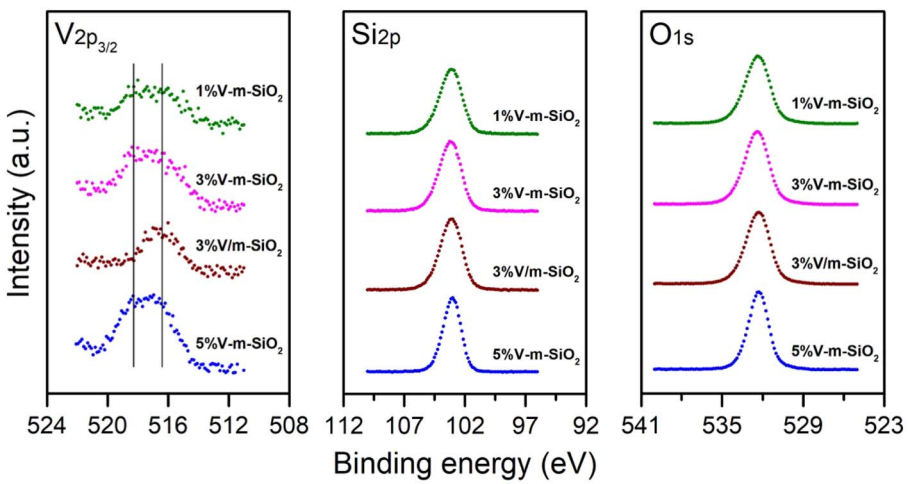


Fig. 5 $V_{2p}$, $Si_{2p}$, and $O_{1s}$ XPS spectra of series of *x*% V-m-$SiO_2$ catalysts and supported 3% V-m-$SiO_2$ catalyst.

$V_{2p3/2}$ region mainly exhibit two peaks at ~518.3 eV and ~516.4 eV, respectively, which correspond to highly-dispersed vanadia species interacting strongly with silica and normal vanadia species with +5 valence.[16,36–39] It is worth noting that the highly-dispersed vanadia species interacting strongly with silica are dominated in *x*% V-m-$SiO_2$ catalyst prepared using a modified sol–gel method, even when vanadium content increases to 5%, the percentage of these species remain be larger than 50%. The reliability of this treatment further is supported by the results of UV-vis DRS measurements, in which two different kinds of $V^{5+}$ species are coexistent. However, for the 3% V/m-$SiO_2$ catalyst prepared by traditional impregnation method, only one XPS peak appears at ~516.4 eV, while no peak assigned to highly-dispersed vanadia species interacting strongly with silica is observed at higher position of binding energy. Combing the previous results, we can conclude that the modified sol–gel method promotes the interaction between the vanadia species and silica support, which will be beneficial for enhancing the reactivity and stability of these catalysts.

### 3.3 Catalytic performance in oxidative dehydrogenation of propane

The catalytic performances in oxidative oxidation of propane over series of *x*% V-m-$SiO_2$ catalysts as well as referenced 3% V m$^{-1}$-$SiO_2$ catalyst are presented in Fig. 6 and 7. Initially, the catalytic activity of vanadium-free m-$SiO_2$ support was measured. There is an extremely low the conversion of propane (no shown), while incorporating vanadium into the m-$SiO_2$ matrix (*x*% V-m-$SiO_2$) enhances the conversion of propane (Fig. 6a), indicating that vanadium are the active components to activate propane. With increasing vanadium content from 1% to 5%, one can see that the conversion of propane exhibits a linear rise from 3.9% to 19.8%. To further reveal the intrinsic activity of vanadium species, we evaluated the specific site rate ($TOF_{C_3H_8}$) of converting propane by calculating the millimoles of propane converted per mole of V per second ($s^{-1}$). *In situ* Raman spectroscopy measurements (Fig. 4a) have confirmed that vanadium exists as a monomeric [$VO_4$] species in series of *x*% V-m-$SiO_2$ catalysts, and correspondingly we assume that all vanadium elements in these catalysts participate in converting process of propane. As presented in Fig. 6a, the $TOF_{C_3H_8}$ values are almost constant with an increase of vanadium content, suggesting that these monomeric [$VO_4$] species isolated into m-$SiO_2$ are the catalytically active sites for the conversion of propane. Also, the dependence of the converting rate of propane ($mol_{C_3H_8}$ $g_{cat}^{-1}$ $h^{-1}$) on the number of active [$VO_4$] sites (vanadium content) can be used to quantitatively determine the number of catalytic active sites involved in the rate-determining-step of propane conversion.[40] A slope of ~1

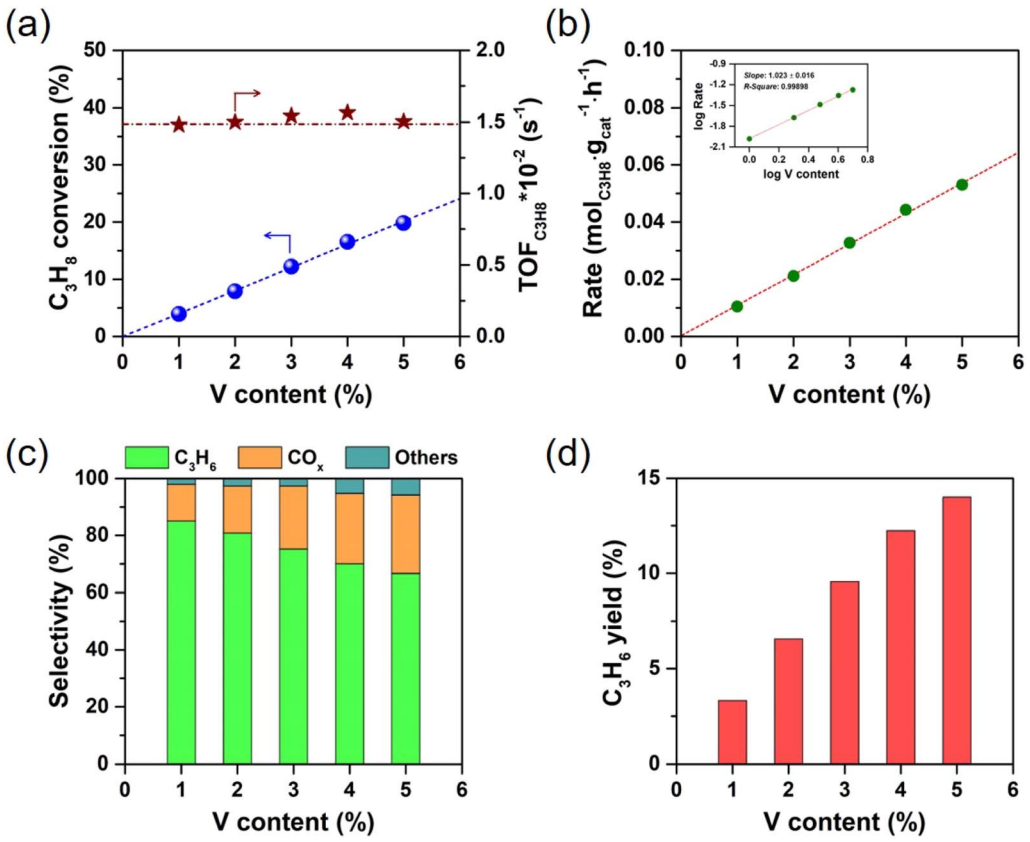


Fig. 6 Catalytic performances in oxidative dehydrogenation of propane plotted as a function of vanadium content over *x*% V-m-$SiO_2$ catalysts prepared using a modified sol–gel method: (a) propane conversion and $TOF_{C_3H_8}$; (b) rates of propane activation, inset: plot of log rate *vs.* log *V* content; (c) product selectivities; (d) yields to propylene (reaction conditions: reaction temperature, 500 °C; catalyst weight, 0.1 g; 16.8 kPa $C_3H_8$, 16.8 kPa $O_2$, $N_2$ balance; gas-hourly-space-velocity, 36 000 mL $g_{cat}^{-1}$ $h^{-1}$).

 

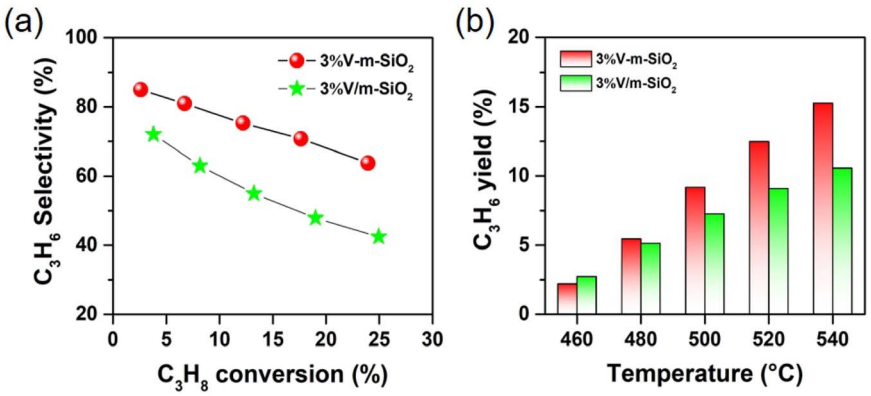


Fig. 7 (a) Propylene selectivity plotted as a function of propane conversion and (b) yield to propylene plotted as a function of reaction temperature over representative 3% V-m-$SiO_2$ catalyst and referenced 3% V/m-$SiO_2$ catalyst (reaction conditions: reaction temperature, 460–540 °C; catalyst weight, 0.1 g; 16.8 kPa $C_3H_8$, 16.8 kPa $O_2$, $N_2$ balance; gas-hourly-space-velocity, 36 000 mL $g_{cat}^{-1}$ $h^{-1}$).

(Fig. 6b) suggests that one [$VO_4$] site is involved in the rate-determining-step of propane activation, further supporting the conclusion that isolated [$VO_4$] species are catalytically active sites in propane conversion.

As shown in Fig. 6c, the product slate consists of propylene, carbon oxides ($CO_x$ including CO and $CO_2$), and others (ethylene, methane, oxygenates) in oxidative dehydrogenation of propane over series of $x$% V-m-$SiO_2$ catalysts. As exemplified by 1% V-m-$SiO_2$ catalyst, propylene is the main product with the selectivity close to 85%, while $CO_x$ is main by-products with a selectivity of ~13% when the conversion of propane approaches 3.9%. With further increasing vanadium content to 5% (5% V-m-$SiO_2$), the selectivity to propylene appears a continuous decrease from 85.1% to 66.7%, accompanied by an obvious increase in the selectivity of $CO_x$ from 12.9% to 27.5%. As is well established in the literature, propylene is the primary product of propane oxidation, and $CO_x$ is formed as a secondary product from the further oxidation of propylene.[41] The current decrease in propylene selectivity with increasing vanadium content may be related to the secondary reaction. Furthermore, the yields for propylene as a function of vanadium content are shown in Fig. 6d to evaluate the catalytic efficacy of $x$% V-m-$SiO_2$ catalysts prepared by the modified sol–gel method. We can see that the yield of target product propylene has a continuous rise, accompanied by a slowing down process when the content exceeds 3%, indicating an intensification of secondary reaction.

To reveal unique behaviors of our catalyst case in propane oxidative dehydrogenation reaction, Fig. 7a further compares the variation of the selectivity to propylene in oxidative dehydrogenation of propane on representative 3% V-m-$SiO_2$ and referenced 3% V/m-$SiO_2$ catalysts at the same scale of vanadium content. Apparently, the 3% V-m-$SiO_2$ catalyst possesses higher selectivity to propylene at both low and high propane conversion levels than those on supported 3% V $m^{-1}$-$SiO_2$ catalyst, suggesting a highly selective nature of the $x$% V-m-$SiO_2$ catalyst prepared using a modified sol–gel method for oxidative dehydrogenation of propane. It is noted that a propylene selectivity of up to 70% at a high propane conversion of 20% could be achieved over the 3% V-m-$SiO_2$ catalyst. For a heterogeneous catalyst, its catalytic performances are strongly dependent on reaction temperature. Fig. 7b further compares the ability of propylene formation on representative 3% V-m-$SiO_2$ catalyst and referenced 3% V/m-$SiO_2$ catalyst at the temperature between 450 °C and 650 °C. It is found that the 3% V-m-$SiO_2$ catalyst shows a poorer yield to propylene at a reaction temperature of 460 °C in comparison to referenced 3% V/m-$SiO_2$ catalyst, but with increasing in reaction temperature, the yields to propylene increase rapidly. At 540 °C, the yield to propylene over the 3% V-m-$SiO_2$ catalyst exceeds 15%, whereas over referenced 3% V/m-$SiO_2$ catalyst, the yield only has 10%. Furthermore, we correlate the structure of active sites with the catalytic behaviors. It is noticeable that using a modified sol–gel method evidently improves the dispersing state of active vanadium species in mesoporous silica. In addition to influencing the dispersion, more importantly, an interaction between vanadium species and silica is enhanced by using a modified sol–gel method to prepare $x$% V-m-$SiO_2$ catalysts. These enhancements on both geometric and electronic properties rendered by the unique sol–gel preparation method thereby boosts the catalytic efficacy of oxidative dehydrogenation of propane to propylene.

## 4. Conclusion

In conclusion, a series of vanadium oxide incorporated mesoporous silica (V-m-$SiO_2$) catalysts is designed and synthesized using a modified sol–gel method. The characterization studies confirm that vanadium oxide exists as monomeric [$VO_4$] species containing one terminal V=O bond and three V–O–Si bonds until atomic ratio of vanadium to silicon approaches to 5%, whereas for vanadium oxide supported mesoporous silica (V/m-$SiO_2$) prepared using a traditional impregnation method, the local aggregation of vanadium oxide species occurs with atomic ratio of vanadium to silicon reaches 3%. It is also verified that a modified sol–gel method not only improves the dispersing state of vanadium oxide in mesoporous silica, and more evidently enhances an interaction of vanadium oxide with

mesoporous silica. Compared to a supported V/m-$SiO_2$ counterpart, present V-m-$SiO_2$ catalyst prepared using a modified sol–gel method exhibits more superior ability to catalyze oxidative dehydrogenation of propane to propylene. Such enhancement on catalytic performances in our case can be reasonably attributed, in part, to its favorable geometric and electronic properties rendered by the unique preparation method.

## Conflicts of interest

There are no conflicts to declare.

## Acknowledgements

The authors acknowledge the financial support from Fundamental Research Program for Young Scientists of Shanxi Province (Project No. 202103021223294).

## References

1 J. J. H. B. Sattler, J. Ruiz-Martinez, E. Santillan-Jimenez and B. M. Weckhuysen, Catalytic dehydrogenation of light alkanes on metals and metal oxides, *Chem. Rev.*, 2014, **114**, 10613–10653.

2 Y. Shan, Z. Sui, Y. Zhu, J. Zhou, X. Zhou and D. Chen, Boosting size-Selective hydrogen combustion in the presence of propene using controllable metal clusters encapsulated in zeolite, *Angew. Chem., Int. Ed.*, 2018, **57**, 9770–9774.

3 S. Sokolov, M. Stoyanova, U. Rodemerck, D. Linke and E. V. Kondratenko, Comparative study of propane dehydrogenation over V-, Cr-, and Pt-based catalysts: Time on-stream behavior and origins of deactivation, *J. Catal.*, 2012, **293**, 67–75.

4 A. S. Bodke, D. A. Olschki, L. D. Schmidt and E. Ranzi, High selectivities to ethylene by partial oxidation of ethane, *Science*, 1999, **285**, 712–715.

5 R. Grabowski, Kinetics of oxidative dehydrogenation of $C_2$-$C_3$ alkanes on oxide catalysts, *Catal. Rev.: Sci. Eng.*, 2006, **48**, 199–268.

6 M. D. Argyle, K. Chen, A. T. Bell and E. Iglesia, Effect of catalyst structure on oxidative dehydrogenation of ethane and propane on alumina-supported vanadia, *J. Catal.*, 2002, **208**, 139–149.

7 F. Cavani, N. Ballarini and A. Cericola, Oxidative dehydrogenation of ethane and propane: How far from commercial implementation?, *Catal. Today*, 2007, **127**, 113–131.

8 J. T. Grant, J. M. Venegas, W. P. McDermott and I. Hermans, Aerobic oxidations of light alkanes over solid metal oxide catalysts, *Chem. Rev.*, 2018, **118**, 2769–2815.

9 R. G. Carraza, C. Peres, J. P. Bernard, M. Ruwet, P. Ruiz and B. Delmon, Catalytic synergy in the oxidative dehydrogenation of propane over MgVO Catalysts, *J. Catal.*, 1996, **158**, 452–476.

10 Y. M. Liu, Y. Cao, N. Yi, W. L. Feng, W. L. Dai, S. R. Yan, H. Y. He and K. N. Fan, Vanadium oxide supported on mesoporous SBA-15 as highly selective catalysts in the oxidative dehydrogenation of propane, *J. Catal.*, 2004, **224**, 417–428.

11 Q. L. Liu, J. M. Li, Z. Zhao, M. L. Gao, L. Kong, J. Liu and Y. C. Wei, Design, synthesis and catalytic performance of vanadium-incorporated mesoporous silica KIT-6 catalysts for the oxidative dehydrogenation of propane to propylene, *Catal. Sci. Technol.*, 2016, **6**, 5927–5941.

12 B. Solsona, T. Blasco, J. M. L. Nieto, M. L. Peña, F. Rey and A. Vidal-Moya, Vanadium oxide supported on mesoporous MCM-41 as selective catalysts in the oxidative dehydrogenation of alkanes, *J. Catal.*, 2001, **203**, 443–452.

13 E. V. Kondratenko, O. V. Buyevskaya and M. Baerns, Characterization of Vanadium-Oxide-Based Catalysts for the Oxidative Dehydrogenation of Propane to Propene, *Top. Catal.*, 2001, **15**, 175–180.

14 A. A. Lemonidou, L. Nalbandian and I. A. Vasalos, Oxidative dehydrogenation of propane over vanadium oxide based catalysts: Effect of support and alkali promoter, *Catal. Today*, 2000, **61**, 333–341.

15 C. Carrero, M. Kauer, A. Dinse, T. Wolfram, N. Hamilton, A. Trunschke, R. Schlogl and R. Schomacker, High performance (VOx)n–(TiOx)m/SBA-15 catalysts for the oxidative dehydrogenation of propane, *Catal. Sci. Technol.*, 2014, **4**, 786–794.

16 Q. L. Liu, Z. Yang, M. S. Luo, Z. Zhao, J. Y. Wang, Z. Xie and L. Guo, Vanadium-containing dendritic mesoporous silica nanoparticles: Multifunctional catalysts for the oxidative and non-oxidative dehydrogenation of propane to propylene, *Microporous Mesoporous Mater.*, 2019, **282**, 133–145.

17 C. A. Carrero, R. Schloegl, I. E. Wachs and R. Schomaecker, Critical literature review of the kinetics for the oxidative dehydrogenation of propane over well-defined supported vanadium oxide catalysts, *ACS Catal.*, 2014, **4**, 3357–3380.

18 C. Hess, J. D. Hoefelmeyer and T. D. Tilley, Spectroscopic characterization of highly dispersed vanadia supported on SBA-15, *J. Phys. Chem. B*, 2004, **108**, 9703–9709.

19 I. E. Wachs, Catalysis science of supported vanadium oxide catalysts, *Dalton Trans.*, 2013, **42**, 11762–11769.

20 J. T. Grant, C. A. Carrero, A. M. Love, R. Verel and I. Hermans, Enhanced two-dimensional dispersion of Group V metal oxides on silica, *ACS Catal.*, 2015, **5**, 5787–5793.

21 A. Khodakov, B. Olthof, A. T. Bell and E. Iglesia, Structure and catalytic properties of supported vanadium oxides: support effects on oxidative dehydrogenation reactions, *J. Catal.*, 1999, **181**, 205–216.

22 B. Schimmoeller, Y. Jiang, S. E. Pratsinis and A. Baiker, Structure of flame-made vanadia/silica and catalytic behavior in the oxidative dehydrogenation of propane, *J. Catal.*, 2010, **274**, 64–75.

23 C. A. Carrero, C. J. Keturakis, A. Orrego, R. Schomacker and I. E. Wachs, Anomalous reactivity of supported $V_2O_5$ nanoparticles for propane oxidative dehydrogenation:

influence of the vanadium oxide precursor, *Dalton Trans.*, 2013, **42**, 12644–12653.

24 Y. M. Liu, W. L. Feng, T. C. Li, H. Y. He, W. L. Dai, W. Huang, Y. Cao and K. N. Fan, Structure and catalytic properties of vanadium oxide supported on mesocellulous silica foams (MCF) for the oxidative dehydrogenation of propane to propylene, *J. Catal.*, 2006, **239**, 125–136.

25 Y. C. Lou, H. C. Wang, Q. H. Zhang and Y. Wang, SBA-15-supported molybdenum oxides as efficient catalysts for selective oxidation of ethane to formaldehyde and acetaldehyde by oxygen, *J. Catal.*, 2007, **247**, 245–255.

26 M. Nadjafi, P. M. Abdala, R. Verel, D. Hosseini, O. V. Safonova, A. Fedorov and C. R. Müller, Reducibility and dispersion influence the activity in silica-supported vanadium-based catalysts for the oxidative dehydrogenation of propane: the case of sodium decavanadate, *ACS Catal.*, 2020, **10**, 2314–2321.

27 C. J. Brinker, Y. F. Lu, A. Sellinger and H. Y. Fan, Evaporation-induced self-assembly: nanostructures made easy, *Adv. Mater.*, 1999, **11**, 579–585.

28 B. Z. Tian, X. Liu, B. Tu, C. Z. Yu, J. Fan, L. Wang, S. Xie, G. D. Stucky and D. Y. Zhao, Self-adjusted synthesis of ordered stable mesoporous minerals by acid–base pairs, *Nat. Mater.*, 2003, **2**, 159–163.

29 L. Shi, X. Q. Zhu, Y. Su, W. Z. Weng, H. Feng, X. D. Yi, Z. X. Liu and H. L. Wan, Synergetic effect of $VO_x$ and $TeO_x$ species in mesoporous $SiO_2$ on selective oxidation of propane to acrolein, *J. Catal.*, 2013, **307**, 316–326.

30 D. Y. Zhao, J. L. Feng, Q. S. Huo, N. Melosh, G. H. Fredrickson, B. F. Chmelka and G. D. Stucky, Triblock copolymer syntheses of mesoporous silica with periodic 50 to 300 angstrom pores, *Science*, 1998, **279**, 548–552.

31 X. T. Gao, S. R. Bare, B. M. Weckhuysen and I. E. Wachs, In Situ Spectroscopic Investigation of Molecular Structures of Highly Dispersed Vanadium Oxide on Silica under Various Conditions, *J. Phys. Chem. B*, 1998, **102**, 10842–10852.

32 D. E. Keller, T. Visser, F. Soulimani, D. C. Koningsberger and B. M. Weckhuysen, Hydration effects on the molecular structure of silica-supported vanadium oxide catalysts: A combined IR, Raman, UV–vis and EXAFS study, *Vib. Spectrosc.*, 2007, **43**, 140–151.

33 H. B. Zhu, S. Ould-Chikh, H. L. Dong, I. LIorens, Y. Saih, D. H. Anjum, J.-L. Hazemann and J.-M. Basset, $VO_x/SiO_2$ catalyst prepared by grafting $VOCl_3$ on silica for oxidative dehydrogenation of propane, *ChemCatChem*, 2015, **7**, 3332–3339.

34 S. Dzwigaj, M. Matsuoka, M. Anpo and M. Che, Evidence of three kinds of tetrahedral Vanadium (V) Species in VSiβ zeolite by diffuse reflectance UV—visible and photoluminescence spectroscopies, *J. Phys. Chem. B*, 2000, **104**, 6012–6020.

35 B. Roman, C. Libor, S. Michal and C. Pavel, DR UV–vis study of the supported vanadium oxide catalysts, *J. Phys. Chem. C*, 2011, **115**, 12430–12438.

36 N. K. Nag and F. E. Massoth, ESCA and gravimetric reduction studies on $V/Al_2O_3$ and $V/SiO_2$ catalysts, *J. Catal.*, 1990, **124**, 127–132.

37 D. Dutoit, M. Schneider, P. Fabrizioli and A. Baiker, Vanadia–silica mixed oxides. Influence of vanadia precursor, drying method and calcination temperature on structural and chemical properties, *J. Mater. Chem.*, 1997, **7**, 271–278.

38 C. Hess, G. Tzolova-Muller and R. Herbert, The influence of water on the dispersion of vanadia supported on silica SBA-15: A combined XPS and Raman study, *J. Phys. Chem. C*, 2007, **111**, 9471–9479.

39 Y. L. Wu, Z. F. Han, X. Yan, W. Z. Lang and Y. J. Guo, Effective synthesis of vanadium-doped mesoporous silica nanospheres by sol-gel method for propane dehydrogenation reaction, *Microporous Mesoporous Mater.*, 2022, **330**, 111616.

40 C. L. Zhao and I. E. Wachs, Selective oxidation of propylene to acrolein over supported $V_2O_5/Nb_2O_5$ catalysts: An in-situ Raman, IR, TPSR and kinetic study, *Catal. Today*, 2006, **118**, 332–343.

41 E. V. Kondratenko, M. Cherian, M. Baerns, D. S. Su, R. Schlögl, X. Wang and I. E. Wachs, Oxidative dehydrogenation of propane over V/MCM-41 catalysts: comparison of $O_2$ and $N_2O$ as oxidants, *J. Catal.*, 2005, **234**, 131–142.